CHEMISTRY OF MATERIALS

Article

pubs.acs.org/cm

Precise Control of Nanohoneycomb Ordering over Anodic Aluminum Oxide of Square Centimeter Areas

Clement K. Y. Ng* and Alfonso H. W. Ngan

Department of Mechanical Engineering, The University of Hong Kong, Pokfulam Road, Hong Kong, People's Republic of China

Supporting Information

ABSTRACT: Large-area nanoporous anodic aluminum oxide (AAO) films with well-controlled pore ordering are highly desirable for making nanotechnological devices with consistent performance. We report here a novel method to precisely control the ordering of the AAO pores over unprecedented large areas in the square millimeter to square centimeter range. Our experiments show that AAO films grown on large [001]-oriented Al grains in oxalic acid exhibit ideal close packing, whereas those grown on [101] grains do not show any resemblance to close packing. Other orientations give rise to intermediate pore ordering. Thus, through careful conditioning of the orientation of the Al substrate, the AAO pore ordering can be actively controlled, and this method should enable systematic and industrial-scale exploitation of the AAO properties versus pore ordering.

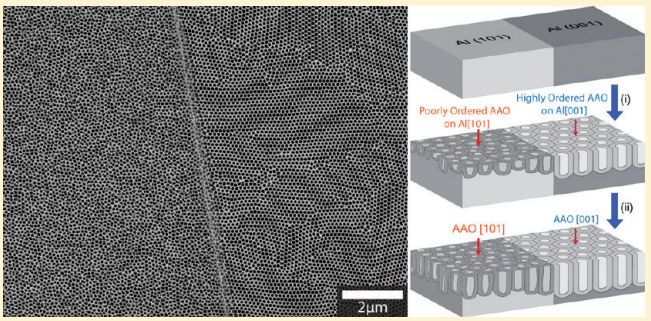

KEYWORDS: *anodic aluminum oxide, grain orientation, characterizations, nanoindentation, nanostructures, nanoporous materials*

INTRODUCTION

Anodic aluminum oxide (AAO) films with a self-ordered, nanoporous honeycomb structure can be formed by controlled electrochemical oxidation of aluminum (Al) surfaces.[1−5] AAO is an important material for a variety of nanotechnological applications because its unique nanoporous honeycomb structure can act as a template for the fabrication of other nanostructured materials.[6−11] Other suggested applications of AAO include electrode support for supercapacitors,[12] microreactors for the catalytic production of hydrogen from ammonia,[13] membranes for high-flow-rate electroosmotic pumps,[14] and gas and environment sensors.[15,16] The recent discovery of a "hard anodization" approach[17] to fabricate AAO at a rate of about 25−30 times faster than that used conventionally should also enhance the industrial-scale exploitation of this structure. However, systematic utilization of AAO would require the spatial ordering of the pore channels to be controllable and homogeneous over large areas. Although the dependence of the AAO pore-channel ordering on the various processing conditions has been widely studied,[3−5,18−23] undesirable variations in the pore ordering between AAO films produced under similar conditions, or within the same film, often remain.[1,19,21,23−26] Surprisingly, in these previous attempts, the grain size and crystallographic orientation of the Al substrate were not explored as potential factors, or have been concluded to be insignificant,[27] in affecting the quality of the AAO films, despite the fact that mature techniques for the grain size and orientation control of Al have long been established.[28−30] In this report, we demonstrate that under identical electrolyte−voltage−temperature anodizing conditions, the grain size and crystallographic orientation of the underlying Al substrate have overriding effects on the quality of the AAO film grown on top. Our results show that, by careful conditioning of the Al substrate, the ordering of the AAO pore channels can be controlled over very large film areas.

EXPERIMENTAL SECTION

AAO films thicker than 100 μm were grown using a procedure based on the conventional two-step oxalic acid anodization (0.3 M, 40 V at 17 °C).[3,19,20] The key difference from the conventional protocol, however, is that before anodization the Al substrate was purposely treated thermomechanically [see Section S1 in the Supporting Information (SI) for details] to achieve grains millimeters to centimeters in size by recrystallization. A number of thermomechanical treatment routes were used to produce different Al substrates for anodization (details are given in the SI), and it was found that recrystallized and electropolished Al substrates with large, equiaxed grains can enable the relationship between the crystallographic orientation of the substrate and the quality of the AAO film grown on top to be clearly elucidated. The results presented here were obtained on Al substrates produced from route C in the SI, and the experimental details can also be found there. On such an Al substrate, the AAO film grown using the two-step anodization method appears as a smooth and transparent film through which the grain structure of the underlying substrate can be seen clearly under an optical microscope (Figure 1a), or even by the naked eye. The darker regions in Figure 1a were found to be lower basins and the brighter regions higher plateaus, implying that the anodizing rate on different Al grains

Received: August 18, 2011
Revised: October 19, 2011
Published: November 7, 2011

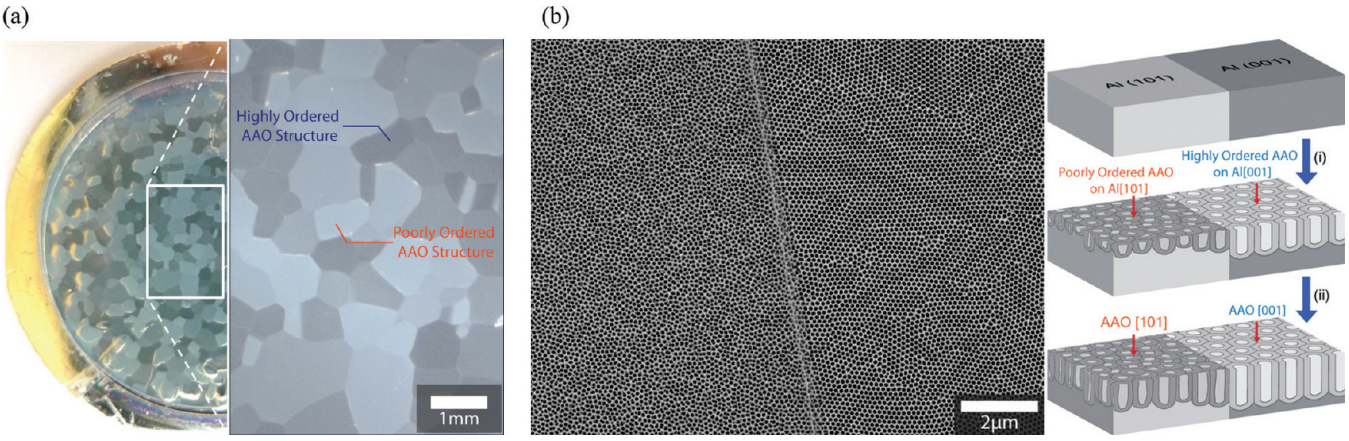

Figure 1. Overall view of the AAO structures: (a) Optical image showing an overview of the as-grown AAO film on the recrystallized, coarse-grained Al substrate. The AAO grown on different Al grains shows different optical contrast, as can be seen more clearly from the magnified view on the right. (b) SEM micrograph of the plane-view AAO structure grown on top of two neighboring Al grains separated by a grain boundary. The AAO on top of the Al grain on the left exhibits very poor spatial ordering of the pores, whereas that on the grain on the right shows high ordering. Subsequent analysis (see the text and Figure 2) shows that the Al grain on the left had a [101] ND, while that on the right had [001]. The 3D morphology of the AAO structure here is illustrated by the schematic diagram on the right.

was different. A scanning electron microscopy (SEM) investigation (Figure 1b) revealed that the AAO structures on neighboring Al grains were very different in terms of the spatial ordering of the pore channels: the pore channels on the left (plateau) grain were poorly ordered, whereas those on the right (basin) grain were highly ordered.

RESULTS AND DISCUSSION

In order to determine quantitatively the degree of spatial ordering of the AAO structures, their radial distribution functions (RDFs) [see Section S2 in the SI] were computed based on the pore-channel positions in their SEM images, and Figure 2a shows five examples in descending order of pore-channel ordering. The leftmost situation in Figure 2a is a highly ordered AAO structure exhibiting a series of distinctive sharp RDF peaks corresponding well to those in an ideal close-packed (ICP) situation. In this situation, the first 10 nearest-neighbor (N−N) separations in the ICP structure can be identified from the experimental RDF, and in the SEM image, the pores are seen to organize into crystalline domains on the order of a few tens of pore spacings. On the other hand, the rightmost situation in Figure 2a is a poorly ordered structure, and its RDF attenuates rapidly to a smooth background beyond the third peak. In this case, even the second or third ICP N−N cannot be unambiguously identified, and in the SEM image, the pore arrangement is random without any resemblance to the ICP. The other cases shown in Figure 2a exhibit intermediate pore ordering. To obtain a quantitative measure of the degree of ordering, the area between the RDF and a background curve fitted to join the troughs of the RDF was computed (see Figure S3 in the SI). This area, termed the "RDF peak intensity" hereafter, was found to vary by about 5 times from 6.38×10^{-5} to 3.01×10^{-4} for all of the structures studied. (The unit here is arbitrary but is a constant for all of the results presented.) In the following, the RDF peak intensities are expressed as normalized values based on the maximum value of 3.01×10^{-4}. The RDF peak intensity correlates well with the visually observed spatial ordering of the different AAO structures in Figure 2a.

The substrate grain orientation was measured by electron backscattered diffraction (EBSD) after dissolving the top AAO layer by a phosphochromic acid solution, as shown in Figure 2b (see Section S2 and Figure S4 in the SI). As shown in the example in Figure 2b, the underlying Al grain in a basin region on which highly ordered AAO was formed (cf. Figure 1a) had a normal direction (ND) close to [001], whereas another grain in a plateau region corresponding to poorly ordered AAO had a normal direction close to [101]. Altogether 101 grains were analyzed, and their normalized RDF peak intensities are plotted against the substrate orientation in Figure 2c. The results indicate that AAO grown on Al grains close to [001] consistently has the highest spatial ordering, whereas that grown on Al close to [101] shows the worst ordering. It is worth noting that AAO grown on orientations near [111] showed surprisingly intermediate ordering, which implies that the planar density of the substrate atoms is not a major determining factor for ordering of the AAO films. The difference in height between the basin and plateau regions of the metal surface after removal of the AAO film was measured by a profiler to be around 12−16 μm after 10 + 10 h of anodization, whereas the thickness of the AAO film was around 150−200 μm. This indicates that the migration speed of the oxide−metal interface depends on the metal orientation.

Figure 3a shows a cross-sectional transmission electron microscopy (TEM) image illustrating the longitudinal view of the top part of the AAO pore-channel structure grown on two neighboring Al grains with [001] and [101] orientations (see Section S3 and Figure S5 in the SI for details of specimen preparation). Selected-area electron diffraction on the AAO structures on the two grains indicates that they are amorphous in nature. Tallying with the plane-view observations in Figure 2c, the corresponding cross-sectional AAO structures on the two grains in Figure 3a had very different ordering: In the AAO structure on the left [101] grain, the pore channels have a high tendency to tilt, merge, and branch as they grow into the underlying metal. In the oxide structure on the right [001] grain, the pore channels tend to grow straight along the film ND (the z direction), without merging or branching. Similar observations are also seen near the metal−oxide interface in Figure 3b, indicating that the pore-channel morphology was essentially the same at an equilibrium state over a growth process of more than 100 μm thick. Thus, any theory that describes the initial regularity of the oxide pits or the

dx.doi.org/10.1021/cm202461z | Chem. Mater. 2011, 23, 5264−5268

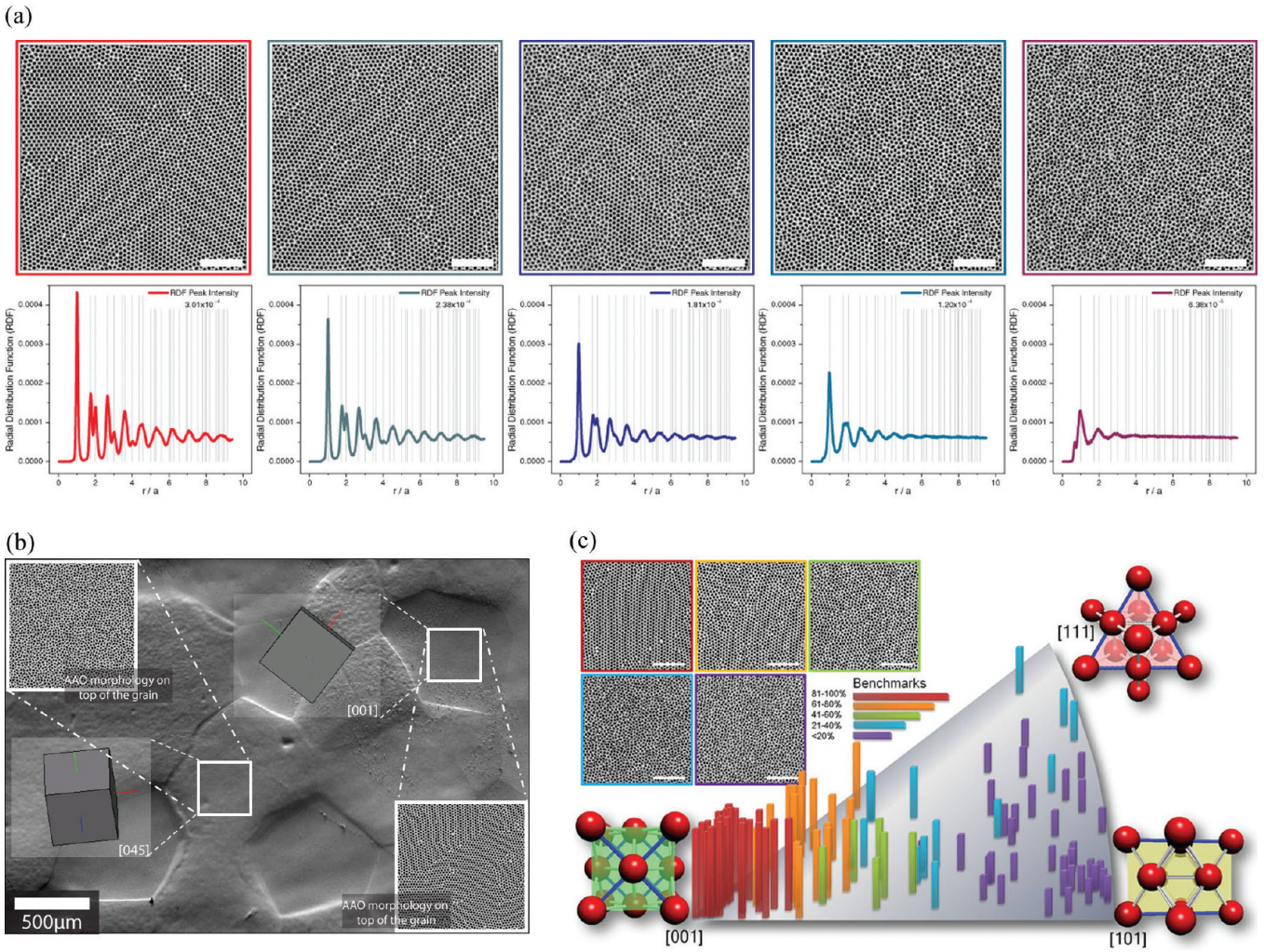

Figure 2. Relationship between pore-channel ordering and Al substrate orientation: (a) SEM images of representative AAO structures and the corresponding RDFs of their pores. The scale bars in the SEM images represent 1 μm. The example on the left has high spatial ordering of the pore channels, and the example on the right has poor spatial ordering. The vertical gray lines in the background of the RDFs represent the structure of an ICP structure for direct comparison. (b) Typical EBSD results of the orientation of the underlying Al metal substrate, after removal of the covering AAO layer. The lower, basinlike grain shown was underneath a highly ordered AAO structure, and its ND is close to [001]. The higher, plateaulike grain shown was underneath a poorly ordered AAO structure, and its ND is close to [045]. The basins and plateaus in the topography of the metal substrate after removal of the covering AAO also corresponded closely to those of the AAO before its removal. (c) Plot of the normalized RDF peak intensities (see the text) of various AAO structures versus their substrate ND in the [001]−[101]−[111] unit triangle of the stereographic projection. The data of 101 grains are shown, and their normalized RDF peak intensities are binned into five categories: 81−100% (red), 61−80% (orange), 41−60% (green), 21−40% (blue), and 0−20% (purple). Representative AAO structures in these five categories are shown in the insets: the specific cases shown have normalized RDF peak intensities of 98% [001] (red), 63% [216] (orange), 48% [113] (green), 29% [045] (blue), and 20% [506] (purple).

undulation of the oxide surface in the early stage of oxidation[31] cannot explain the eventual regularity of the oxide pattern for oxide films that are >100 μm thick. Note that, in the two-step anodizing procedure used here, the initial oxidation pits do not necessarily bear any relation to the plane-view pore channels of the eventual oxide product because an initially grown oxide layer was dissolved away, leaving only the dimples at the metal surface as seeds for the second anodizing step. The fact that the initial pits are more regularly or irregularly arranged on the x−y plane sheds little light on explaining why these pits eventually develop into >100-μm-long pore channels, which in some cases are straight but in other cases are tilted with frequent merging and branching.

It is important to realize that the present observations were made on single anodizing experiments of polycrystalline Al substrates (cf. Figure 1a) and so the difference in the AAO ordering cannot be explained by variations in the overall anodizing conditions, in terms of the acid medium, applied voltage, or temperature, between experiments. Clearly, the only factor that is substantially different between the very different AAO ordering observed is the orientation of the Al substrate grain. The substrate orientation effect was studied in a previous report,[27] but that study focused on the effects of misorientations between a few grains rather than on how the orientation of the substrate grains determines the AAO ordering in a quantitative way. Nevertheless, it is interesting to note that the grain orientations encountered in ref 27, namely, [−111], [203], and [011] and [−317], [031], and [021], correspond to the poor-to-intermediate AAO ordering regime according to our present findings; therefore, the orientation effects in that

dx.doi.org/10.1021/cm202461z | Chem. Mater. 2011, 23, 5264−5268

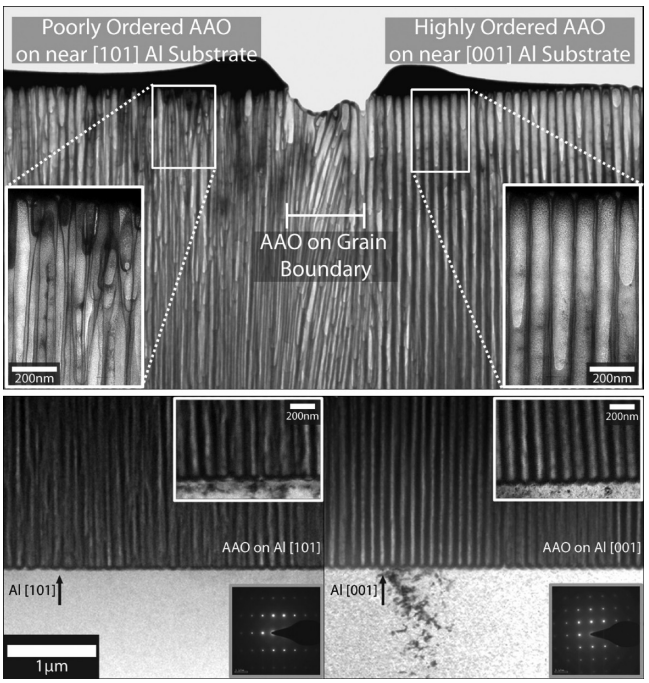

Figure 3. Cross-sectional TEM micrographs showing the longitudinal morphology of the AAO: (a) Cross section near the top surface of the AAO film. (b) Cross section at the metal−oxide junction. The structure shown is grown on top of a grain-boundary region in the Al substrate. The two Al grains on either side of the grain boundary had [001] and [101] orientation, respectively.

case may not be discernible visually, and unfortunately no quantitative measure of the AAO ordering was provided in that study.

It is known that upon oxidization Al undergoes a volume expansion that is believed to be relieved primarily by oxide flow, and this has been suggested as a reason for self-ordering of the AAO structure.[23,32] The elastic anisotropy of the substrate can unlikely explain the observed dependence of the AAO ordering on substrate orientation by affecting the oxide flow, as a simple analysis will show. Because the ND (denoted as the z direction hereafter) is less constrained during the film growth process, the constraints by the substrate are mainly due to Al's elastic constants along the in-plane x and y directions, i.e., the sum $c_{1111}' + c_{2222}'$, where the elastic constants c_{ijkl}' refer to the $x-y-z$ coordinate system of the oxide film. For z along [001], [101], or [111], $c_{1111}' + c_{2222}'$ equals $2c_{11}$, $2c_{11} + H/2$, or $2c_{11} + 5H/6$, respectively, where c_{ij} here refer to the cubic axes of the Al unit cell and $H = 2c_{44} + c_{12} - c_{11}$ is the anisotropy factor (ref 33, p 434). Thus, if elastic anisotropy plays a significant role, one would expect the order of the oxide pattern to change along the sequence [001], [101], and [111]. However, the regularity of the oxide pattern is observed to decrease in a different sequence, [001] > [111] > [101]. Moreover, Al is actually a very isotropic material elastically, with $H/2c_{11}$ equal to only ~5% (ref 33, p 837). Such a small anisotropy in the in-plane elasticity of the underlying metal is unlikely to be important in affecting the growth of the oxide pore channels at the metal−oxide interface. However, the density of the oxide formed on differently oriented grains may not be the same, and this may be a factor for the observed dependence of pore ordering on substrate orientation. Finally, electropolishing[25,26] is known to produce different surface conditions on different crystal orientations, but we have also carried out control experiments using vibratory polishing instead of electropolishing to produce mirror-finished Al substrates. AAO ordering and quality after the two-step anodization were found to be identical with electropolishing for the same grain orientation. This shows that the surface pretexture prior to two-step anodization is unlikely a controlling factor for AAO ordering, but the substrate grain orientation is.

CONCLUSION

In summary, the present work illustrates a method, namely, conditioning of the underlying Al substrate, to produce large areas of AAO with homogeneous and controlled spatial ordering. The recrystallized Al substrates of purity >99.99% in Figures 1−3 had grain sizes of a few millimeters, and as described in the SI, recrystallization of ultrahigh-purity (>99.9999%) Al can result in grain sizes up to a few centimeters, and again the AAO grown on top was still homogeneous in structure. If specially grown single crystals of Al are used as substrates, a further increase in the AAO film area with homogeneous pore ordering is possible. This should open up opportunities for systematic exploitation into the various properties of AAO as a function of pore ordering. As an indication, the hardness of two AAO structures on [001] and [101] Al, with RDF peak intensities of 89% and 27%, respectively, was found to be very different at 1300 ± 100 and 800 ± 100 MPa, respectively (see Section S4 and Figure S6 in the SI for details). This is not unexpected because, in a poorly ordered structure, local stresses exhibit big variations about their mean-field values, and so the probability of encountering extremely large stresses that trigger damage increases.[34,35] It is very likely that other physical or chemical properties of AAO can also change significantly with respect to the spatial ordering. Future research should also focus on the mechanism of the present observed substrate dependence of the pore ordering. It is known that Al undergoes a volume expansion upon oxide formation, and this has been suggested as a reason for self-ordering of the AAO structure.[23,32] The density of the oxide may change on different oriented substrates, and this may be an important factor for variation of the self-ordering tendency of the AAO.

ASSOCIATED CONTENT

Supporting Information

Materials and methods in this work, substrate treatment and anodizing procedures, quantitative determination of the spatial ordering of AAO films, TEM sample preparation, and nanoindentation experiments on the AAO films. This material is available free of charge via the Internet at http://pubs.acs.org.

AUTHOR INFORMATION

Corresponding Author

*E-mail: kycng@hku.hk.

ACKNOWLEDGMENTS

We thank Prof. B. J. Duggan for kindly providing the Al slabs used in this study and suggesting the conditions for recrystallization. The work described in this paper was supported by grants from the Research Grants Council (Project HKU7156/08E), as well as from the University Grants Committee (Project SEG-HKU06) of the Hong Kong Special Administration Region, People's Republic of China. A.H.W.N.

acknowledges support in the form of a Senior Research Fellowship from the Croucher Foundation. We also thank C. Cheng for helpful discussions.

REFERENCES

(1) Thompson, G. E.; Furneaux, R. C.; Wood, G. C.; Richardson, J. A.; Goode, J. S. *Nature* **1978**, *272*, 433−435.
(2) Thompson, G. E.; Wood, G. C. *Nature* **1981**, *290*, 230−232.
(3) Masuda, H.; Fukuda, K. *Science* **1995**, *268*, 1466−1468.
(4) Masuda, H.; Hasegwa, F.; Ono, S. *J. Electrochem. Soc.* **1997**, *144*, L127−L130.
(5) Masuda, H.; Yamada, H.; Satoh, M.; Asoh, H.; Nakao, M.; Tamamura, T. *Appl. Phys. Lett.* **1997**, *71*, 2770−2772.
(6) Hu, W. C.; Gong, D. W.; Chen, Z.; Yuan, L. M.; Saito, K.; Grimes, C. A.; Kichambare, P. *Appl. Phys. Lett.* **2001**, *79*, 3083−3085.
(7) Zhang, Y.; Li, G. H.; Wu, Y. C.; Zhang, B.; Song, W. H.; Zhang, L. *Adv. Mater.* **2002**, *14*, 1227−+.
(8) Zheng, M. J.; Zhang, L. D.; Zhang, X. Y.; Zhang, J.; Li, G. H. *Chem. Phys. Lett.* **2001**, *334*, 298−302.
(9) Sander, M. S.; Prieto, A. L.; Gronsky, R.; Sands, T.; Stacy, A. M. *Adv. Mater.* **2002**, *14*, 665−667.
(10) Sander, M. S.; Gronsky, R.; Sands, T.; Stacy, A. M. *Chem. Mater.* **2003**, *15*, 335−339.
(11) Li, Y.; Cheng, G. S.; Zhang, L. D. *J. Mater. Res.* **2000**, *15*, 2305−2308.
(12) Chen, Q. L.; Xue, K. H.; Shen, W.; Tao, F. F.; Yin, S. Y.; Xu, W. *Electrochim. Acta* **2004**, *49*, 4157−4161.
(13) Ganley, J. C.; Seebauer, E. G.; Masel, R. I. *AIChE J.* **2004**, *50*, 829−834.
(14) Vajandar, S. K.; Xu, D. Y.; Markov, D. A.; Wikswo, J. P.; Hofmeister, W.; Li, D. Y. *Nanotechnology* **2007**, 18.
(15) Varghese, O. K.; Gong, D. W.; Dreschel, W. R.; Ong, K. G.; Grimes, C. A. *Sens. Actuators, B* **2003**, *94*, 27−35.
(16) Varghese, O. K.; Grimes, C. A. *J. Nanosci. Nanotechnol.* **2003**, *3*, 277−293.
(17) Lee, W.; Ji, R.; Gosele, U.; Nielsch, K. *Nat. Mater.* **2006**, *5*, 741−747.
(18) Masuda, H.; Yada, K.; Osaka, A. *Jpn. J. Appl. Phys., Part 2* **1998**, *37*, L1340−L1342.
(19) Li, A. P.; Muller, F.; Birner, A.; Nielsch, K.; Gosele, U. *J. Appl. Phys.* **1998**, *84*, 6023−6026.
(20) Li, F. Y.; Zhang, L.; Metzger, R. M. *Chem. Mater.* **1998**, *10*, 2470−2480.
(21) Nielsch, K.; Choi, J.; Schwirn, K.; Wehrspohn, R. B.; Gosele, U. *Nano Lett.* **2002**, *2*, 677−680.
(22) Shingubara, S.; Morimoto, K.; Sakaue, H.; Takahagi, T. *Electrochem. Solid State Lett.* **2004**, *7*, E15−E17.
(23) Jessensky, O.; Muller, F.; Gosele, U. *Appl. Phys. Lett.* **1998**, *72*, 1173−1175.
(24) Parkhutik, V. P.; Shershulsky, V. I. *J. Phys. D: Appl. Phys.* **1992**, *25*, 1258−1263.
(25) Konovalov, V. V.; Metzger, R. M.; Zangari, G. *Proc. Electrochem. Soc.* **2000**, *99−34*, 203−208.
(26) Konovalov, V. V.; Zangari, G.; Metzger, R. M. *Chem. Mater.* **1999**, *11*, 1949−1951.
(27) Lu, B.; Bharathulwar, S.; Laughlin, D. E.; Lambeth, D. N. *J. Appl. Phys.* **2000**, *87* (9), 4721−4723.
(28) Dillamore, I. L.; Katoh, H. *Met. Sci.* **1974**, *8*, 73.
(29) Hirsch, J.; Nes, E.; Lücke, K. *Acta Metall.* **1987**, *35*, 427.
(30) Hjelen, J.; Ørsund, R.; Nes, E. *Acta Metall. Mater.* **1991**, *39*, 1377.
(31) Singh, G. K.; Golovin, A. A.; Aranson, I. S. *Phys. Rev. B* **2006**, 73.
(32) Houser, J. E.; Hebert, K. R. *Nat. Mater.* **2009**, *8*, 415−420.
(33) Hirth, J. P.; Lothe, J. *Theory of Dislocations*, 2nd ed.; Krieger Publishing Co.: Malabar, FL, 1992.
(34) Ngan, A. H. W. *Proc. R. Soc. London, Ser. A* **2005**, *461*, 433−458.
(35) Ngan, A. H. W. *Proc. R. Soc. London, Ser. A* **2005**, *461*, 1423−1446.